Procedia Manufacturing

Volume 1, 2015, Pages 663–674

43rd Proceedings of the North American Manufacturing Research Institution of SME http://www.sme.org/namrc

Effect of Cutting Edge Geometry on Thermal Stresses and Failure of Diamond Coated Tools

Jamal Sheikh-Ahmad[1] and Parikshit Chipalkati[2]

[1]*The Petroleum Institute, Abu Dhabi, U.A.E*

[2]*Cessna India, Bengaluru, Karnataka, India*

jahmad@pi.ac.ae, parikshitchipalkatti@yahoo.com

Abstract

This study considers the residual thermal stresses induced by cooling in diamond coated carbides after the chemical vapor deposition process. Finite element analysis and simulation of thermally induced residual stresses was conducted using a transient thermo-mechanical coupled solver. Cutting tool geometry parameters including cutting edge angle, nose radius and film thickness were varied and the resulting thermal stresses were analyzed and compared. Both radial and hoop stresses were found to be compressive along the bisector of the cutting edge angle of sharp cutting tools with zero nose radius. Radial stresses were tensile and hoop stresses were compressive for honed tools with large nose radius. It was found that thermal stresses are mainly affected by the ratio of nose radius to film thickness (r/h). But the effect of cutting edge angle was most influential for cutting tools with sharp edges. Increasing the cutting edge angle for these tools generally resulted in an increase in the magnitude of thermal stresses. Qualitative criteria for film fracture was also applied, which revealed that film failure is most likely to occur in thick films and for cutting tools with large cutting edge angles and r/h ratios less than 1.0. Some experimental validation of these criteria was also provided.

Keywords: thermal stresses, diamond film, cutting tool, tungsten carbide substrate, nose radius, film thickness, cutting edge angle.

1 Introduction

The extreme hardness of diamond, its high thermal conductivity and low coefficient of friction make it an ideal material for cutting tools and tool coatings. Therefore, diamond coated carbides are sought after for machining abrasive materials such as medium density fiberboard (MDF) and fiber reinforced polymers (FRPs). However, these tools are known to develop cracks and fail prematurely by brittle film fracture due to the presence of substantial residual stresses in the diamond film. Thermal residual stresses are generated during cooling after the chemical vapor deposition process (CVD) due to mismatches in thermal expansion coefficient of the diamond coating and the carbide substrate. Residual thermal stresses have been recognized as a major driving force for coating failure

Peer-review under responsibility of the NAMRI Scientific Committee

doi:10.1016/j.promfg.2015.09.071

(Gunnars and Alahelisten, 1996; Wiklund, et al., 1999; Clyne, 2001; Vila et al., 2008; Qin et al., 2009). It was pointed out that the presence of high compressive residual stresses in the film, even though beneficial for arresting tensile cracks, may actually cause cracks to deviate their path in a direction parallel to the surface and thus leading to fracture of surface areas of the film (Gunnars and Alahelisten, 1996).

Thermal stresses in the diamond film can be calculated from thermal expansion coefficients of the substrate and diamond. The thermal strain in the diamond film on a fairly large and flat substrate and away from edges can be calculated from

$$\varepsilon_{th} = \int_{T_1}^{T_o} (\alpha_s - \alpha_f) dT \qquad (1)$$

where α_s and α_f are temperature dependent thermal expansion coefficients of the substrate and film, respectively, T_1 is deposition temperature and T_o is room temperature. The resulting thermal stress for plane stain conditions is calculated from

$$\sigma_{th} = \frac{E_f \varepsilon_{th}}{(1-\nu_f)} \qquad (2)$$

where E_f is the film Young's modulus and ν_f is its Poisson's ratio. The state of stress is found to be equal bi-axial state in the plane of the film and away from edges. The stress is also uniform in the thickness of the film. For diamond coatings on carbides it was reported by Gunnars and Alahelisten (1996), Hollman et al. (1995) and Kuo et al. (1996) that the stress is compressive and is of large magnitudes exceeding 2.5 GPa. The total stress in the diamond film is the algebraic summation of intrinsic stresses and the residual thermal stresses (Clyne, 2001; Kuo et al., 1996). Intrinsic stresses arise from crystal growth phenomena, crystal defects, and deposition of non-diamond carbon. Intrinsic stresses in diamond film were found to be tensile and its magnitude varied between 0.2 to 0.6 GPa depending on methane concentration and deposition temperature (Clyne, 2001). Therefore, even though the coated tool has not been used in machining its coating already bears large residual stresses which may lead to coating failure.

The state of stress in complex geometry cutting tools is not necessarily uniform or equally biaxial. Studies conducted by Gunnars and Alahelisten (1996), Qin et al. (2009) and Renaud et al. (2009) on thermal stresses in cutting edges of specified nose radius has indicated that thermal stresses vary across the thickness and around the curvature of the cutting edge. The complex state of stress arising from deposition can't be predicted by equation (2) and numerical solutions were found to work best. These studies have shown that the state of stress around the cutting edge contains compressive tangential stress, tensile radial stress and a shear stress component. The magnitude of these components varies across the thickness of the film and with location around the curvature of the cutting edge. At locations far away from the curvature (more than 500μm away) the state of stress approaches the equal biaxial compressive state found in coatings on a flat substrate (Gunnars and Alahelisten, 1996). Furthermore, the complex state of stress around the curvature of the cutting edge depends greatly on film thickness and cutting edge radius. But a direct correlation between thermal stresses can be found with the ratio of cutting edge radius to film thickness (Gunnars and Alahelisten, 1996).

Studies on machining wood-based composites and fiber reinforced polymers with diamond coated carbides indicated that diamond coated tools exhibited poor performance as compared to the uncoated tools (Usuki, et al., 1991; Sheikh-Ahmad and Morita, 2002; Sheikh-Ahmad, et al., 2003; Köpf et al. 2006). The dominant forms of wear reported in these studies were fracture and delamination of the diamond film as shown in Figure 1. This may have resulted from inadequate adhesion and/or the presence of residual stresses in the film coating and lack of mechanical strength and toughness at the edge, respectively. Figure 1(a) reveals a radial crack at the outer surface of the curved cutting edge

approximately at the bisector of the cutting edge angle. Diamond crystals have been evidently lost at the mouth of the crack and the crack is shown to extend radially through the film thickness. The radial crack at the surface would occur only if a tensile tangential state of stress was present. Figure 1(b) shows gross delamination of the diamond film from the cutting edge nose region. Examination of the fracture surface indicates that the crack did not propagate radially across the entire thickness until reaching the substrate. The crack path appears to have deflected in a direction parallel to the substrate. This crack behavior signifies the presence of a complex state of stress in the diamond film. This type of film failure also confirms a model proposed by Gunnars and Alahelisten (1996). According to this model, asperities at the outer surface of the film cause high stress concentration at the base of protruding crystals, which causes them to break away. Radial cracks may also be introduced as a result. But since the crack is faced with compressive tangential stress as it propagates toward the substrate, it changes its direction following maximum shear stress trajectories. This puts it in a path parallel to the substrate. The intersection of these cracks then leads to removal of a surface area of the film as shown in Figure 1(b).

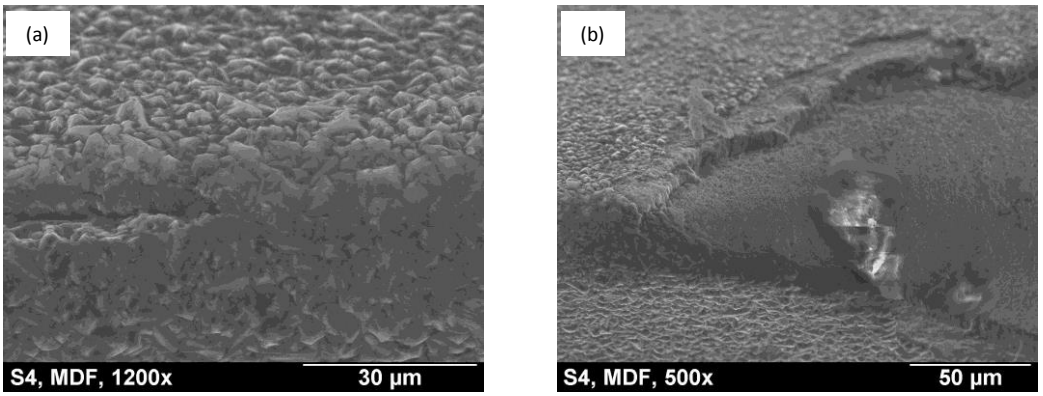

Figure 1 SEM images showing radial crack in the diamond film on the tool nose (a) and in-plane and interfacial delamination of coating also around the nose of the tool (b).

Better understanding of the state of stress in the diamond film at the curved cutting edge and how the film fails would lead to a better design of diamond coated cutting tools. Because of the unique cutting edge geometry used for machining wood and fibrous composites, which requires sharp cutting edges and very small nose radii, the state of stress on this cutting edge geometry is expected to be different from cutting tools used for metal machining, where the cutting edge angle approaches 90^{o} and nose radii are in the order of 500µm. Therefore, the purpose of this study is to investigate the state of thermal stresses in diamond coatings on sharp cutting edges and to identify the effect of cutting edge geometry and film thickness on residual stresses. The aim is to be able to identify optimum cutting edge geometry that will result in lowering the thermal residual stresses.

2 Numerical Simulation of Thermal Stresses

2.1 The cutting tool

The cutting tool used in this study is a cemented carbide insert that is 30 mm long, 12 mm wide, 1.5 mm thick and is made from C3 carbide grade (WC-4% Co). The insert is ground along its length and on both sides to form two cutting edges. The cutting edge angle is typically 55^{o}. Figure 2(a) shows a schematic of the geometry of the cutting insert. The initial cutting edge nose width, as viewed under microscope in a direction along the bisector of the cutting edge included angle, is in the order of 3 to 5

μm. This type of throw-away carbide insert is commonly used in edge trimming of wood based composite panels such as MDF and particleboard. This explains the need for the slender cutting edge and the extreme sharpness that is required to make clean cuts.

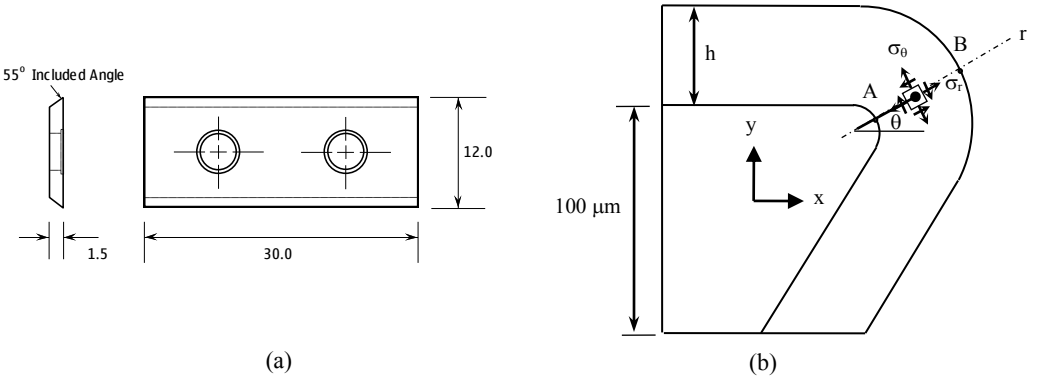

Figure 2 Geometry of carbide insert (a) and finite element model (b)

2.2 Finite element model

Because of the large length of the insert, its middle section may be considered in a state of plane strain due to symmetry around the centerline. Figure 2(b) shows a portion of this section that was utilized for finite element analysis. Only a small portion of the cross section was considered for analysis in order to reduce computation time. The cutting edge geometry was divided into two sections, namely the substrate and the coating as shown in Figure 2(b). Four node 2D plane strain element formulation was used for meshing. Element density at the interface and the outer periphery was kept dense so that to ensure no loss of important stress and temperature gradients, and also it was evident that the smaller the element size the more stable were the stress contours.

Both substrate and coating materials were assumed to be homogenous and isotropic. Since diamond has very high melting temperature and exhibits very little plastic deformation under loading, its mechanical behavior was assumed to be linear-elastic and independent of temperature. Temperature dependent thermal expansion coefficients however were defined for both tungsten carbide and diamond, and temperature dependent yield strength was defined only for tungsten carbide. For this analysis it was assumed that these properties changed in a linear fashion with temperature, thus limiting the number of points required to define the temperature dependence to only two. Other thermal properties such as heat capacity and thermal conductivity were also defined, but were assumed to be independent of temperature. The mechanical and thermal properties for both film and substrate are summarized in Table 1 (Wright et al., 1994).

Symmetry boundary conditions were applied in the plane of the section in Figure 2(b). All the nodes on the left side were constrained in x-translation and y-rotational movement. And all the nodes along the bottom side were constrained in y-translation and x-rotational degree of freedom. This was done to signify the absence of bending loads and clamping force on a free standing insert. Due to the deposition of diamond coating on the substrate, both materials are exposed to a high temperature and eventually air cooled to room temperature after the deposition was done. The tool is assumed to be at stress free condition at time t = 0 sec and all the stress build up is assumed to be due to the cooling (i.e. no intrinsic stress present). All nodes were initially assigned the deposition temperature of 850°C, except for the nodes on the bottom edge, which throughout the simulation were maintained at room temperature (27°C) so as to approximate a condition in which the tool is placed on a cooled tool tray. The coating surface was open for heat transfer to the surrounding by convection. Nonlinear, transient

coupled themo-mechanical analysis was performed to calculate the thermal stresses resulting from cooling.

To avoid mesh dependency of the numerical solution, the finite element model was tested for mesh sensitivity for both sharp and honed coated tools. The mesh density was varied from 800 to 7200 elements. The mesh distribution was kept the same in all analyses (i.e. denser mesh at the interface between the substrate and coating). Comparison of thermal stress results showed that the solution converged at a mesh density of 6000 elements. Therefore, for all subsequent analyses, the mesh density was kept at this level.

Table 1. Mechanical and Thermal Material Properties

Material Properties	**Units**	**Coating**	**Substrate**
Density	$Kg/\mu m^3$	3.50E-15	15E-15
Young's Modulus	$N/\mu m^2$	1050E-03	640E-03
Poisson's Ratio		0.2	0.26
Thermal conductivity	W/m-°K	2000	100
Heat capacity	N-μm/Kg-k	518E+06	130E+06

Temperature Dependent Properties					
		827º	27º	827º	27º
Thermal Expansion coefficient	N-μm/μm-sec-k	2.75E-06	7.50E-07	5.50E-06	4.00E-06
Yield Strength	$N/\mu m^2$	NR		1.40E-04	6.60E-04

2.3 Mechanical loading

Mechanical loading to simulate machining induced stresses in the diamond film was performed independent of the thermo-mechanical analysis assuming that the principle of superposition holds. The coated cutting edge (stress free) was subjected to forces both in the cutting direction and normal to the cutting direction. The magnitude of these forces was determined experimentally from orthogonal turning tests on medium density fiberboard (MDF). The magnitudes of the forces for a depth of cut 0.1 mm and a width of cut of 19 mm were 100 N and 80 N, respectively. In this analysis, and as a first approximation, the cutting edge was indented into the workpiece in a preexisting notch equal to the depth of cut and applying the forces on the fixed end of the cutting edge. The stress distribution in the film was determined as a result of this indentation. This approximation was necessary to avoid the complexity of modeling chip formation in MDF, which is beyond the scope of this work. However, to make this simulation more realistic, the indentation geometry was the same as the geometry of cutting, maintaining the same rake angle and clearance angle relationships as in cutting. Therefore, this simulation approximately represented the indentation stage preceding chip formation in machining.

2.4 Parametric study

Tools with sharp (as received) and honed nose were considered for this study. This was done because previous research by Sheikh-Ahmad et al. (2003) has shown that honing of the cutting edge may improve adhesion strength of the diamond film. Parametric analysis was conducted to analyze the effects of tool geometry on the magnitude and nature of thermal stresses. Edge angle, q, nose radius, r, and coating thickness, h, were varied in three levels each. This resulted in 27 combinations of tool edge geometry and coating thickness. Table 2 lists the levels of each parameter considered in this study. Each of the cases in the parametric study was modeled and analyzed and the thermal stresses resulting from cooling were calculated and compared.

Table 2. Cutting edge geometry combinations for the parametric study

Parameter	Level 1	Level 2	Level 3
Cutting edge angle, q (deg.)	45	55	65
Nose radius, r (μm)	0	10	20
Coating thickness, h (μm)	5	10	20

3 Results and Discussion

3.1 Thermal stress distribution

Figure 3 shows representative contours of the von-Mises thermal stresses in the cutting tool for the combination of q = 55°, r = 20μm and h = 10μm. Similar plots were obtained for all the other tool combinations in this study but were omitted for brevity. It can be seen from this figure that gigantic thermal stresses (in the order of 4 GPa) are generated in the diamond film. Thermal stresses are clearly affected by the curvature of the nose of the cutting edge. At locations far enough from this curvature and from the edges the stress in the film is uniform. It was shown by Gunnars and Alahelisten (1996) that this far field stress actually conforms to the theoretical stress estimated by equation (2) for a large and flat coated area. Within the curvature of the nose of the cutting tool, sharp gradients of stress exist and the stress field is axisymmetric. The maximum stresses and the greatest stress gradients occur along the line bisecting the cutting edge angle. Therefore, all subsequent stress analysis is performed along the bisector. The symmetry of the stress field around the bisector has also been confirmed by the findings of Gunnars and Alahelisten (1996), Qin et al. (2009) and Renaud et al. (2009).

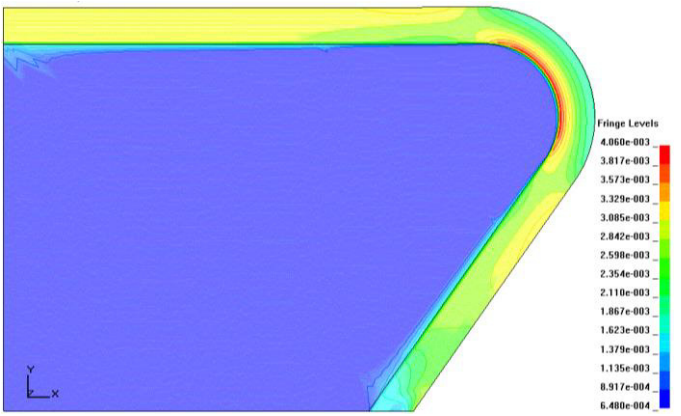

Figure 3. Contours of von-Mises stress (N/μm^2) for cutting tool with 55^o edge angle, 20μm nose radius and 10μm coating thickness.

Thermal stresses along the bisector of the cutting edge are obtained by transforming stresses from the local (x,y) coordinates to the polar (r,θ) coordinates using the usual 2-D stress transformation equations as shown in Figure 2(b). Figure 4 shows the variation of the radial, tangential and shear stresses in the film and substrate along line AB for cutting edge angle of 55^o and different combinations of film thickness and nose radius. Similar plots were obtained for the other cutting edge angles used in this study. It can be seen from Figure 4(c) that the magnitudes of the shear stress along the bisector is negligible when compared to the radial and hoop stresses, which supports the notion

that the state of stress in the curvature zone is axisymmetric and that the polar coordinates are also the directions of the principal stresses.

Figure 4(a) shows that the radial stresses in the substrate are generally tensile and almost constant in the order of 1.0 GPa for rounded edges. For a sharp edge the substrate stress is tensile at the far field and becomes compressive approaching the interface. Similarly, the film radial stress at the interface was tensile for rounded edges and compressive for the sharp edge. Approaching the free surface of the film the radial stresses approached zero as expected. The magnitude of the radial stress at the interface is largely determined by the cutting edge nose radius. For sharp edges the interfacial radial stress was compressive and large whereas it was tensile and smaller for larger nose radii. The transition in the state of stress from the interface to the free surface depended largely on the interaction between nose radius and film thickness. For sharp edges the radial stresses were always compressive. However, for nose radius of 10μm and coating thicknesses of 10 and 20 μm, the radial stress transitioned from tensile to compressive and finally to zero as the location was traversed from interface to the free surface. For all other combinations the radial stress remained tensile in the film.

Figure 4(b) shows that the hoop stress in the substrate is of small magnitude and generally tensile at locations away from the interface. The hoop stresses in the film are always compressive and large at the interface and transition to tensile as the location reaches the free surface for most combinations of cutting tools. The location at which the hoop stress becomes tensile depends both on nose radius and coating thickness. For sharp cutting edges the hoop stress always transitions from compressive to tensile approximately halfway through the thickness. For larger nose radii, transition occurs only for film thicknesses larger than 5μm. Knowing that cracks in the diamond film propagate in tensile stress fields, it becomes apparent that the transition in the hoop stress is favorable for Mode I crack propagation from the surface and toward the substrate. However, as the crack propagates towards the interface past the point of transition it is faced by increasing compressive hoop stresses and tensile or compressive radial stress. This will result in deflecting the crack path to follow the trajectory of the maximum shear stress and cracks may propagate under Mode II fracture below the surface. This results in delamination of large areas of the diamond film as shown in Figure 1(b).

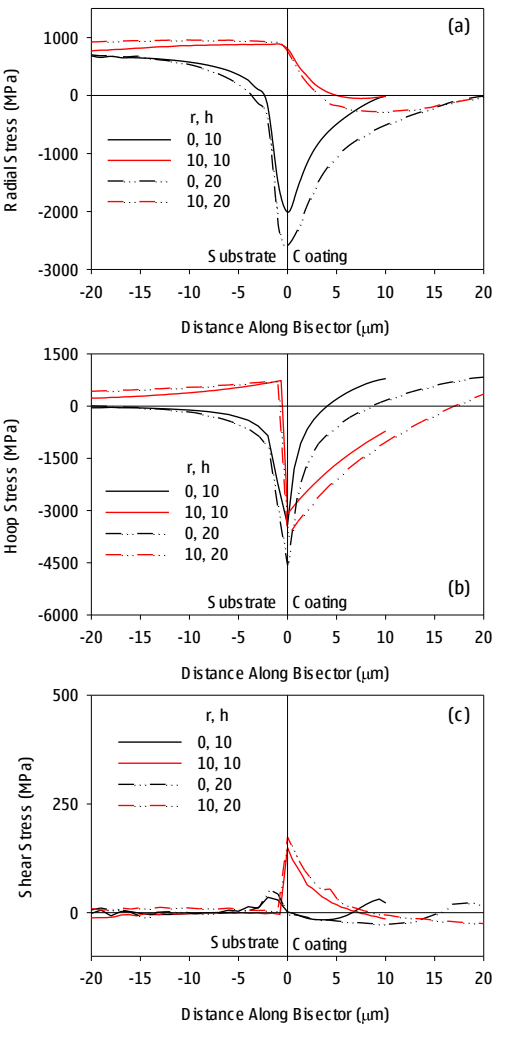

Figure 4. Variation of thermal stresses in the substrate and film along the bisector of cutting edge angle of 55°.

3.2 Effect of r/h ratio on thermal stresses

It is apparent from the previous discussion that the three geometry parameters, cutting edge angle, nose radius and coating thickness, interactively affect the state of thermal stresses in the film. To better understand the effect of tool geometry and film thickness on the magnitude and nature of thermal stresses generated along the bisector of the cutting edge, we consider the effect of the ratio of nose radius to film thickness (r/h) as a way to combine the effect of these two parameters. Figure 5 shows the variation of the three components of thermal stress with (r/h) for the three cutting edge angles considered.

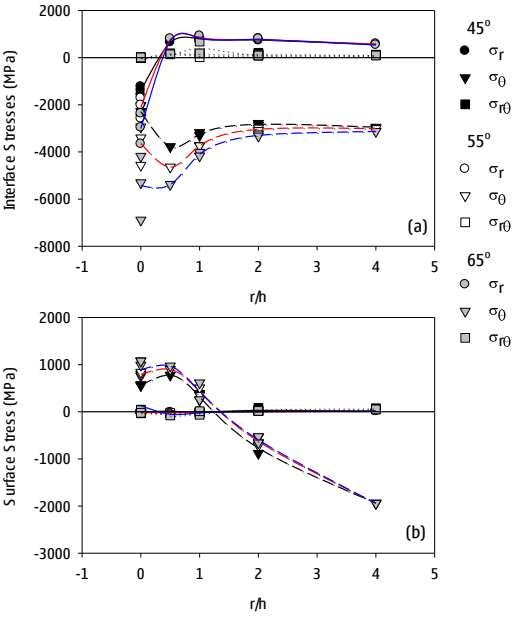

Figure 5. Variation of thermal stresses with (r/h) ratio, (a) at the interface point A and (b) at the surface point B.

Figure 5(a) shows the variation of thermal stresses at the interface (point A in Figure 2(b)) for different values of (r/h). It can be seen that the state of stress at the interface is almost independent of cutting edge geometry for (r/h) ratios greater than 1.5. For lower values of this ratio, the cutting edge angle becomes very influential in determining the state of the stress at the interface. The influence of the cutting edge angle is seen to be the greatest for nose radius of 0μm. Because the shear stress is negligible, the state of stress in the thickness of the film at the interface is biaxial with unequal stresses. For (r/h) less than 0.25 both stresses are compressive and large. For greater (r/h) values the hoop stress is compressive and large while the radial stress is tensile and much smaller in magnitude.

Figure 5(b) shows the variation of thermal stresses on the free surface of the film (point B in Figure 2(b)) with (r/h) ratio. This figure shows that the state of stress at the surface is influenced the most by (r/h) ratio and that the effect of cutting edge angle is not as significant as in the case of the interfacial stress. Furthermore, it is seen that both radial stress and shear stress are insignificant as compared to the hoop stress. In other words, the state of stress at the surface is almost a uniaxial state of stress in the hoop direction. The magnitude of the hoop stress at the surface is much smaller than that at the interface. Because of the sensitivity of Mode I crack propagation to tensile stress, it is of great significance to note that the transition from tensile to compressive hoop stress occurs approximately at (r/h) = 1.25. Furthermore, larger values of (r/h) (thinner diamond films and/or larger nose radii) promote extremely high compressive stresses while smaller values of (r/h) (thicker films and/or smaller nose radii) produce tensile stresses, which are favorable for radial crack initiation and propagation at the free surface of the film as shown in Figure 1(b).

3.3 Stresses from mechanical loading

The stresses in the coating due to mechanical loading are shown in Figure 6 as a function of distance in the film thickness along the bisector. The results are shown only for selective tool geometries as an example. Results for remaining geometries were similar. The figure shows that mechanical stresses in the film due to indentation are generally very small in comparison with the thermal stresses. The radial stresses are compressive and increase in magnitude only slightly as the location is traversed along the bisector from interface to free surface. The hoop stresses are also compressive, but their magnitude increases more significantly by traversing from the interface to the

free surface. The shear stresses are much smaller than the other two components. Because of the small magnitude of mechanical stresses as compared to thermal stresses, it is safe to assume that thermal stresses are the driving force of film failure. Once a crack is generating either due a manufacturing defect or due to mechanical loading at surface asperities, the environment in the film would promote its growth leading to gross film failure. Therefore, strategies for improving coating performance should focus on managing thermal stresses in the film.

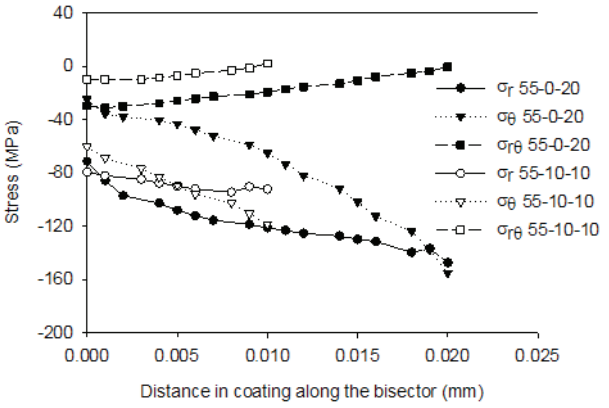

Figure 6. Mechanical stresses across the diamond film thickness along the bisector.

3.4 Film failure criteria

Film failure might be caused by three modes, namely fracture due to excessive tensile stresses (Mode I), shearing (Mode II) and buckling due to compressive stresses. Thus it is necessary to identify the critical areas where the film is most likely to fail by one or more of these failure modes. Based on the results from previous analyses, it was decided that the bisector of the cutting edge would be the most likely location for these three types of stresses to exist. Large compressive hoop stresses at the interface may lead to buckling while large tensile hoop stresses at the free surface may lead to radial cracking. In between these two locations the biaxial state of stress would produce large shear stresses which may lead to crack propagation in directions other than radial and tangential. These three cases are examined below.

Stresses in the diamond film are made of the algebraic sum of intrinsic stress, thermal stress and mechanical stress,

$$\sigma_f = \sigma_i + \sigma_{th} + \sigma_m \qquad (3)$$

Clyne (2001) observed that intrinsic stresses in hot filament CVD diamond film are tensile and in the order of 0.4 to 0.6 GPa, depending on deposition temperature and methane gas concentration. The mechanical stresses from indentation, as discussed in section 3.3 were found to be compressive and maximum at the coating surface. The largest mechanical stress for 20μm film was in the order of 0.12 GPa in the hoop direction. The state of thermal stress at the free surface of the coating is equal biaxial with either tensile or compressive hoop stress, depending on (r/h) ratio as shown in Figure 5(b).

Fracture of thin films under the different modes discussed above and for the complex geometry and stress fields presented here is difficult to analyze. Therefore, criteria for fracture for an infinitely wide film as predicted by linear elastic fracture mechanics is adopted as a conservative first approximation as proposed by Suo (2001). For film fracture under tension the critical stress for fracture is given by

$$\sigma_{cs} = \frac{K_{IC}}{\beta\sqrt{a}} \qquad (4)$$

where β is a constant depending on crack geometry and a is crack length. K_{IC} is fracture toughness for Mode I and it is in the range from 3.0 to 9.0 MPa.m$^{-1/2}$, depending on film quality (Drory, 1995; Kamiya, et al., 1997; Telling and Field, 1998). Assuming that a crack of length equal to the film thickness and β = 3.94 for a crack in an infinite plate, the critical stress for different film thicknesses

can be calculated using eq. (4). Figure 7(a) shows the ratio of the total surface hoop stress to critical stress for fracture for different values of (r/h). An average fracture toughness of 6.0 MPa.m$^{-1/2}$ was used in the calculations. Film failure by surface cracking is likely to occur for stress ratios of 1.0 or greater. The total hoop stress at the surface is found to be more than the critical stress for fracture for (r/h) values less than 1.0 and for film thickness of 20 μm. This makes these tool geometries more susceptible to Mode I fracture at the surface. This is of course a conservative and qualitative assessment because cracks of smaller lengths might be found.

The estimation performed above may also be used for interfacial debonding under Mode II fracture due to maximum shear stress. The interfacial fracture toughness for diamond films was reported by Peng and Clyne (1998) and Kemiya et al. (2002) to be in the range from 14 to 21 MPa.m$^{-1/2}$. The critical shear stress for interfacial fracture was calculated using eq. (4) based on an average value of interfacial fracture toughness and the results are shown in Figure 7(b). Again, it is found that cutting geometries with film thickness of 20 μm are most prone to this mode of failure. The effect of (r/h) ratio is not clear as tools with sharp noses and 20 μm film thickness do not meet this criterion.

For film failure by buckling an interfacial defect of minimum length is required. This allows the film to act as a plate constrained at its ends. Suo (2001) applied Euler's stability principle for columns to this problem and determined the minimum length of the interfacial defect required for buckling, l_c,

$$l_c = \frac{\pi h}{\sqrt{3\left(1-\nu_f^2\right)}}\left(\frac{E_f}{-\sigma}\right)^{1/2} \qquad (5)$$

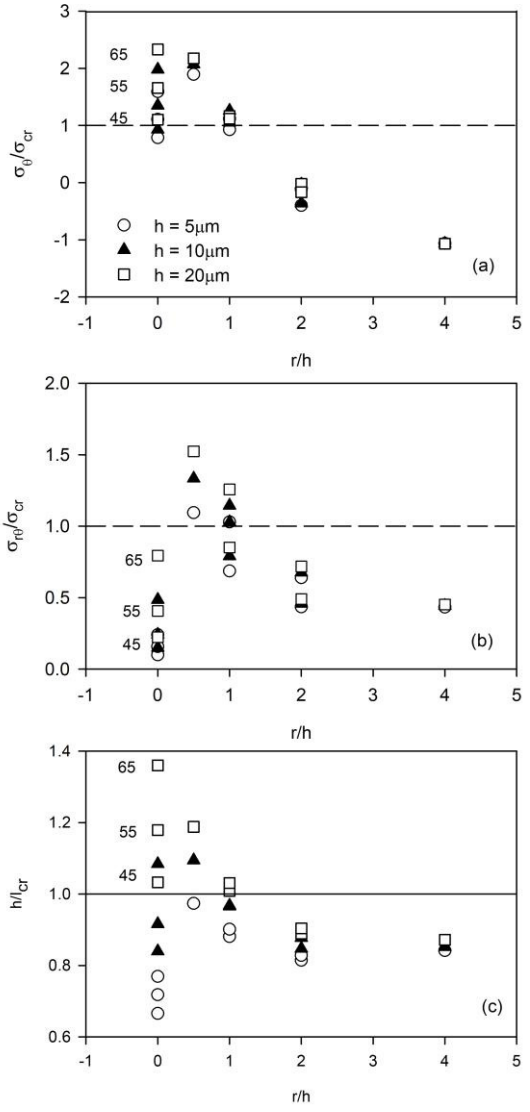

Figure 7. Critical stress for fracture in (a) Mode I, (b) Mode II, and critical interfacial defect length for buckling (c). Numbers refer to cutting edge angles.

where E_f is the coating elastic modulus, h is coating thickness and -σ is the compressive stress acting in the plane of the film (in this case this is the total interfacial hoop stress). Figure 7(c) shows the ratio h/l_c for different values of (r/h). Assuming the presence of interfacial cracks of the same size as the film thickness, buckling would occur for h/l_c ratios of 1 or more. The figure shows that buckling may occur for some tool combinations with (r/h) values of 1 or less and different coating thicknesses. The deciding factor in this mode of failure appears to be the cutting edge angle as most instances of possible failure by buckling have cutting edge angle of 55 or higher and coating thickness of 10 μm or more.

The above analysis is approximate and qualitative in nature due to the lack of exact fracture mechanics criteria for the cutting edge geometries considered. At best, it indicates configurations that are less likely to fail by having lower stresses than the critical stresses. It can be concluded from this analysis that the cutting edge geometry is an influential factor in determining the likelihood of failure of the diamond film. The most consistent outcome from this analysis is that cutting tools with (r/h) ratios greater than 1.0 are less likely to fail by fracture. Furthermore, thinner films and smaller cutting edge angles also reduce the likelihood of film failure by fracture or buckling.

3.5 Experimental results

Some limited experimental validation of the analysis presented above can be found in a previous study by Sheikh-Ahmad et al. (2003). In this work, diamond coated tools were used in machining MDF on a planer. Table 3 shows the geometry of the carbide inserts used in this study. Insert D0 was a sharp insert (as received condition) while inserts D1 and D2 received edge honing by a commercial provider. The carbide inserts were coated with diamond film by a commercial coating provider using a proprietary hot filament CVD process. Details of the experimental setup can be found in the aforementioned reference. Examination of the cutting edges after cutting revealed that insert D0 failed prematurely by gross fracture of the diamond film along the entire cutting edge. Inserts D1 and D2 showed signs of film fracture at isolated locations on the cutting edge only after machining over 1500 lineal meters of MDF. Furthermore, SEM images of insert D2 (Figure 1) show evidence of the formation of radial cracks (Mode I) and surface and interfacial fracture (Mode II). The analytical results in Table 3 show that inserts D0 and D2 are predicted to fail by Mode I fracture, but insert D0 has a higher chance of failure because of the higher hoop stresses in the film. The chances of failure by Mode II fracture for insert D2 and by buckling for inserts D0 and D2 are marginal. The stresses in insert D1are below the critical stresses for fracture for all modes and no failure is predicted.

Table 3. Cutting edge geometry combinations and failure criteria for the experimental study

Insert	Angle	r	h	r/h	Mode I ($\sigma_\theta/\sigma_{cr}$)	Mode II ($\sigma_{r\theta}/\sigma_{cr}$)	Buckling (h/l_{cr})
D0	55	4	15	0.27	1.49	0.35	1.01
D1	55	20	10	2	-0.36	0.68	0.88
D2	55	10	15	0.67	1.39	1.05	1.04

4 Conclusions

Residual thermal stresses in diamond coated tools with different cutting edge geometries were analyzed using the finite element method. Cutting tools with different cutting edge angles, nose radii and film thicknesses were considered. A qualitative fracture criteria by Mode I, Mode II and buckling was also applied. Analysis of residual thermal stresses in these tools indicates that:

1. Stresses around the curvature of the cutting edge are axisymmetric and their state along the bisector of the cutting edge is that of principal stresses (i.e. shear stress is negligible).
2. Thermal stresses in the hoop direction are greater in magnitude than those in the radial direction.
3. For cutting tools with small nose radii, both hoop and radial stresses are compressive at the interface with the substrate while hoop stresses are tensile on the free surface.
4. For cutting tools with large curvature hoop stresses are compressive both at the interface and the free surface. Radial stresses are tensile at the interface.

5. Cutting tools with thicker film thicknesses, smaller nose radii and larger cutting edge angles are more prone to failure by film fracture.
6. Some limited experimental work provided validation of the failure criteria.

References

Clyne TW. Residual stresses in coated and layered systems. In: Buschow KH, Cahn RW, Flemings MC, Ilschner B, Kramer EJ, Mahajan S, Veyssière P, editors. *Encyclopedia of Materials: Science and Technology* (Second Edition), Oxford, Elsevier; 2001, p. 8126-8134.

Drory MD. Fracture of synthetic diamond. *Journal of Applied Physics* 1995; 78: 3083-3088.

Gunnars J and Alahelisten A. Thermal stresses in diamond coatings and their influence on the coating wear and failure. *Surface and Coatings Technology* 1996; 80:303-312.

Hollman P, Alahelisten A, Olsson M and Hogmark S. Residual stress, Young's modulus and fracture stress of hot flame deposited diamond. *Thin Solid Films* 1995; 270: 137-142.

Kamiya S, Kimuraa H, Yamanobe K, Saka M and Abe´ H. A new systematic method of characterization for the strength of thin films on substrates-evaluation of mechanical properties by means of 'film projection'. *Thin Solid Films* 2002; 414: 91-98.

Kamiya S, Sato M, Saka M and Abé H. Fracture toughness estimation of thin chemical vapor deposition diamond films based on the spontaneous fracture behavior on quartz glass substrate. *Journal of Applied Physics* 1997; 82: 6056-6061.

Köpf A, Feistritzer S and Udier K. Diamond coated cutting tools for machining of non-ferrous metals and fibre reinforced polymers. *International Journal of Refractory Metals and Hard Materials* 2006; 24: 354-359.

Kuo CT, Lin CR and Lien HM. Origins of the residual stress in CVD diamond films. *Thin Solid Films* 1996; 290-291: 254-259.

Peng XL and Clyne TW. Mechanical stability of DLC films on metallic substrates Part II - Interfacial toughness, debonding and blistering. *Thin Solid Films* 1998; 312: 219-227.

Qin F, Chou YK, Nolen D and Thompson RG. Coating thickness effects on diamond coated cutting tools. *Surface and Coatings Technology* 2009; 204: 1056-1060.

Renaud A, Hu J, Qin F and Chou K. Numerical simulation of 3D tool geometry effects on deposition residual stresses in diamond coated tools. *International Journal of Mechatronics and Manufacturing Systems* 2009; 2:490-501.

Sheikh-Ahmad J and Morita T. Tool coatings for wood machining: problems and prospects. *Forest Products Journal* 2002; 52: 43-51.

Sheikh-Ahmad J and Sirdhar G. Edge Trimming of CFRP composites with diamond coated tools: edge wear and surface characteristics. SAE Technical Paper 2002-01-1526.

Sheikh-Ahmad J, Stewart JS and Feld H. Failure characteristics of diamond-coated carbides in machining wood-based products. *Wear* 2003; 255: 1433-1437.

Suo Z. Fracture in Thin Films. In: Buschow KH, Cahn RW, Flemings MC, Ilschner B, Kramer EJ, Mahajan S, Veyssière P, editors. *Encyclopedia of Materials: Science and Technology* (Second Edition), Oxford, Elsevier; 2001, p. 3290-3296.

Telling RH and Field JE. Fracture in CVD diamond. *International Journal of Refractory Metals and Hard Materials* 1998; 16: 269-276.

Usuki H, Narutaki N and Yamane Y. A Study of Cutting Performance of Diamond Coated Tools. *International Journal of Japan Society of Precision Engineering* 1991; 25: 35-36.

Vila M, Lopes AB, Almeida FA, Fernandes AJS and Silva RF. Extrinsic stress induced defects in CVD diamond. *Diamond and Related Materials* 2008; 17:190-193

Wiklund U, Gunnars J and Hogmark S. Influence of residual stresses on fracture and delamination of thin hard coatings, *Wear* 1999; 232:262-269

Wright JK, Williamson RL and Maggs KJ. Finite element analysis of the effectiveness of interlayers in reducing thermal residual stresses in diamond films. *Materials Science and Engineering* 1994; A187: 87-96.